

Electronic Supplementary Information

Hybrid organic-inorganic H₂-evolving photocathodes: understanding the route towards high performances organic photoelectrochemical water splitting

Francesco Fumagalli^{a,†}, Sebastiano Bellani^{a,†}, Marcel Schreier^b, Silvia Leonardi^a, Hansel Comas Rojas^a, Ali Ghadirzadeh^a, Gabriele Tullii^a, Alberto Savoini^c, Gianluigi Marra^c, Laura Meda^c, Michael Grätzel^b, Guglielmo Lanzani^a, Matthew T. Mayer^b, Maria Rosa Antognazza^{a,*} and Fabio Di Fonzo^{a,*}

a. Center for Nano Science and Technology @PoliMi, Istituto Italiano di Tecnologia, Via Pascoli 70/3, 20133 Milano, Italy. Address here.

b. Laboratory of Photonics and Interfaces, Institute of Chemical Sciences and Engineering, Ecole Polytechnique Fédérale de Lausanne, CH-1015 Lausanne, Switzerland

c. Eni S.p.A., Istituto ENI Donegani, Via Giacomo Fauser 4, 28100 Novara, Italy.

† These authors contributed equally.

E-mail: fabio.difonzo@iit.it; mariarosa.antognazza@iit.it

For conversions from the measured electrode potential (vs. Ag/AgCl) to the standard RHE (NHE at pH = 0) used through the text for discussion, the following calculation was used.

$$E_{\text{RHE}} = E_{\text{Ag/AgCl}} + 0.059 \cdot \text{pH} + E_{\text{Ag/AgCl}}^0; \quad [E_{\text{Ag/AgCl}}^0 = +0.197 \text{ V}]$$

One important concern about the application of organic semiconductors to water splitting is their stability in water or aqueous solutions. This argument usually develops from observed degradation phenomena in OPV systems exposed to humid environment, showing oxidation of the organic semiconductor/metallic electrode interface. However, a first indication that SP's hold the potential to become materials of choice for photoelectrochemical application evolved from experiments showing that the same conjugated polymer employed in our experiments, (rr-P3HT), fully preserves its optoelectronic capabilities in an aqueous environment (see ref. 12 in the main text), as shown by optical, IR and Raman spectroscopy, as well as its charge generation and recombination dynamics, as shown by transient absorption experiments.

In figure 2 of the text we show linear sweep voltammetry experiments carried out on the FTO/BHJ device operating at +0.18V vs. RHE, which we report here below on a larger scale at the reviewer's commodity (left panel). We completed the characterization of the FTO/BHJ device by carrying out a chronoamperometry measurement. The capacitive spikes present in the chronoamperometry

measurements have been removed for the sake of clarity. One should notice that the measured current is very stable over one hour continuous operation, in exactly the same conditions employed in the main text for the characterization of the device including also the electron- and hole-selective contacts and the catalyst layer. At certain times (minutes 17th and 52nd) the illumination was stopped to show dark current value. This finding fully confirms that the major origin of current decrease observed in the complete device (see Figure 3a and 3c in the main text) cannot be ascribed to the polymer blend layer itself.

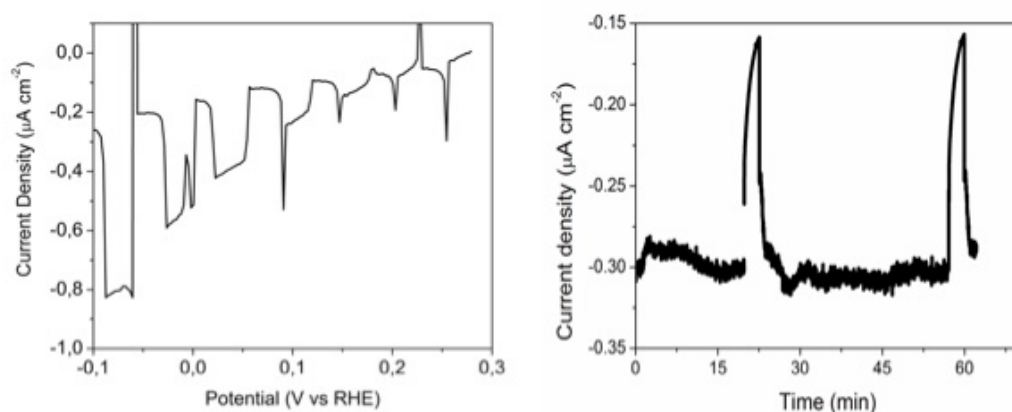


Figure S1. (left panel) Reproduction over a full scale of the FTO/BHJ photocathode current–potential characteristics measured in 0.1 M H₂SO₄-Na₂SO₄ solution at pH 1.37, under chopped AM 1.5 light illumination (100 W cm⁻²) after 60 minutes of polarization at +0.18 V vs RHE (same as Figure 2 in the main text). (Right panel) Photocurrent density in potentiostatic operation for the FTO/BHJ photoelectrode, over one hour continuous operation. At certain times the illumination was chopped to show dark currents. For the sake of clarity, capacitive spikes were removed.

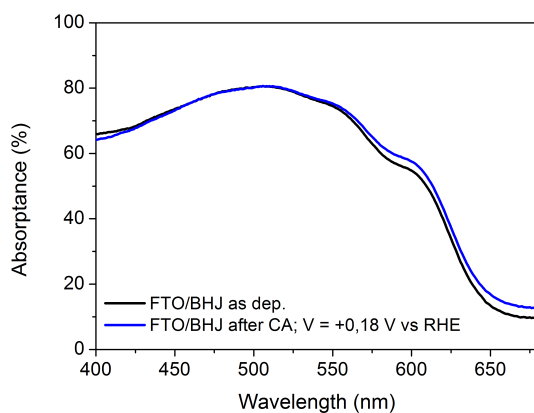


Figure S2. UV-Vis-nIR absorbance spectra of a FTO/BHJ photocathode before (black line) and after (blue line) 60 mins of potentiostatic operation at +0.18 V vs RHE in 0.1 M H₂SO₄-Na₂SO₄ solution at pH 1.37.

Irreversible degradation of the polymer is usually clearly visible as a change in the optical absorption lineshape, as well as a pronounced decrease in the optical absorbance. Figure S2 shows the comparison between the optical absorption acquired before (black line) and after (blue line) chronoamperometry measurements, under the same conditions employed for the characterization of the whole photocathode for hydrogen production. Neither the vibronic sequence, nor the absorption intensity are seriously affected by prolonged functioning in the photoelectrochemical cell upon 1 sun illumination and under external bias, thus indicating negligible irreversible degradation effects of the polymer blend.

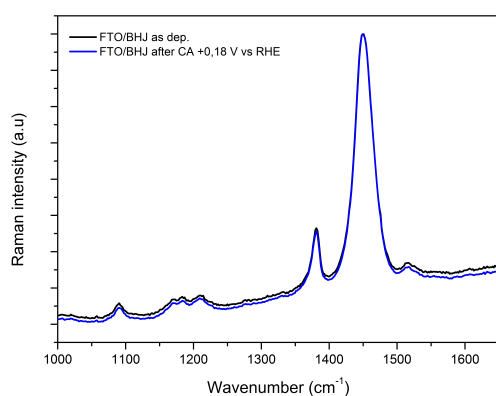


Figure S3a. Resonant Raman absorption spectra of FTO/BHJ devices before (black line) and after (blue line) 1 hour continuous operation at +0.18 V vs RHE in 0.1 M H₂SO₄-Na₂SO₄ solution at pH 1.37.

Raman spectroscopy is another valuable tool to assess polymer stability under prolonged functioning. In order to evaluate the importance of irreversible changes in the p-electron delocalization and possible conjugation break, we measured the resonant Raman spectrum before (black line) and after (blue line) the 1-hour long chronoamperometry scan (Figure S1). The two main peaks at 1378 cm⁻¹ and 1445 cm⁻¹ (assigned to C-C stretching and in-phase C=C/C-C stretching/shrinking of the aromatic thiophene ring) were analyzed in detail, and no differences between the two scans were evidenced, thus allowing to exclude the occurrence of strong irreversible processes. In other words, change in the polymer conjugation length, under the same operating conditions employed in photocathode operation, can be excluded. Strong oxidation of the material can be also ruled out by the absence of a peak around 1624 cm⁻¹, traditionally attributed to a quinoid structure in presence of irreversible processes.

As a further argument we report here (figure S3b) the same measurement described in the paragraph above performed on FTO/BHJ/Pt photocathodes. In this case the presence of the catalysts allowed to operate the system in chronoamperometric mode at much higher current levels (several hundreds of $\mu\text{A cm}^{-2}$ see figure 3c in the main text) providing a more significant environment for materials stability. Also in this situation the semiconducting polymer did not show any variations in its Raman spectrum.

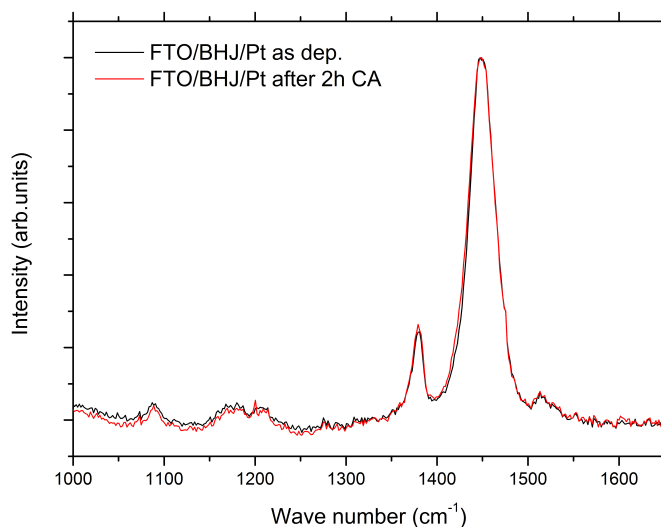


Figure S3b. Resonant Raman absorption spectra of FTO/BHJ/Pt devices before (black line) and after (red line) 2 hours continuous operation at -0.17 V vs RHE in 0.1 M $\text{H}_2\text{SO}_4\text{-Na}_2\text{SO}_4$ solution at pH 1.37.

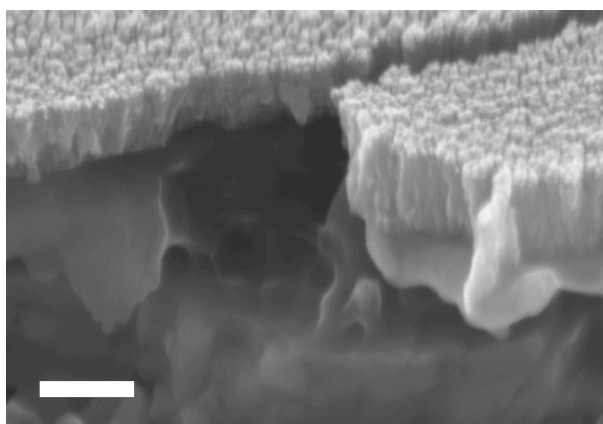


Figure S4. High resolution scanning electron micrograph cross sectional image showing the detailed nanostructured morphology of the TiO_2 electron selective layer deposited on top of the BHJ layer in a FTO/ MoO_3 /BHJ/ TiO_2 /Pt photocathode architecture. Image is taken after thermal treatment of the device and before electrochemical experiments. Scale bar, 100nm.

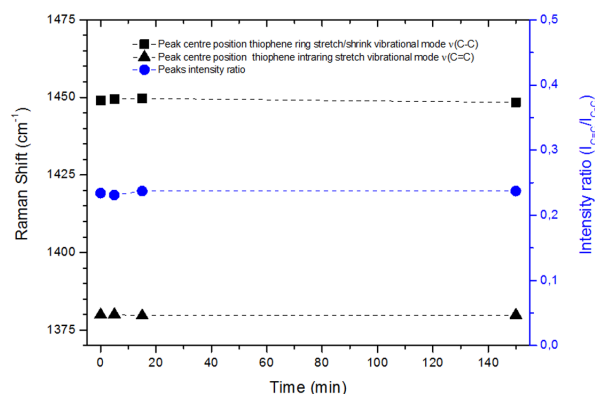


Figure S5. Comparison after different operation times in CA between Raman peaks spectral position and intensity ratio. The Raman spectra were measured on complete photocathodes before and after chronoamperometry. Two peaks were considered (see Fig. 4b in the main text) arising from rr-P3HT molecule vibrational modes involving characteristic thiophene ring π -electron delocalized bonds.

The two main peaks appearing on the raman spectra recorded on the photocathodes at 1379 and at 1449 cm^{-1} have been assigned to aromatic thiophene's in-plane ring skeleton modes, C–C stretching and in phase C=C/C–C stretching/shrinking respectively. The analysis of rr-P3HT degradation during hydrogen evolution operation is focused on these two vibration modes since they are reported to be sensitive to π -electron delocalization (conjugation length) of P3HT molecules as well as to extension of the crystalline domains, moreover literature studies report that the Raman spectra of neutral state oligothiophenes generally show a correlation between the peak positions of the stretching vibrations of the conjugated C=C bonds and the number of repeating units in the polymer chain.

The lack of any significant change in the structure of the selected raman peaks for photocathodes operated for different CA times suggests the absence of major structural and electronical variations within the rr-P3HT film caused by the polymer/electrolyte interaction during the chronoamperometric dynamic behaviour of the device. As a consequence the significant variations in current density and onset potential during CA measurements are addressed to the physical-chemical modification of some other layer in the photocathode architecture.

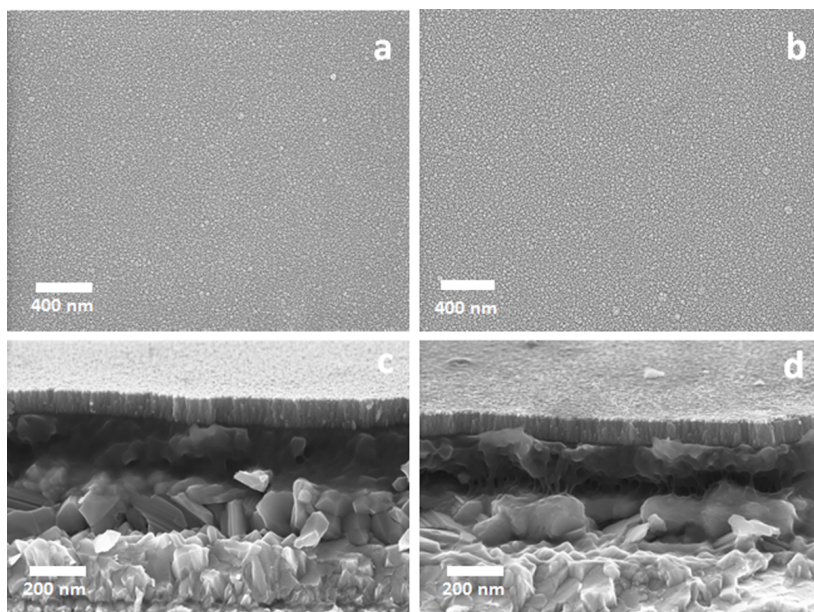


Figure S6. HR-SEM micrographs (top view in the first row and cross sectional view in the second row) of the FTO/MoO₃/P3HT:PCBM/TiO₂/Pt photocathode before (a,c), and after 150 minutes (b,d) of chronoamperometric measurement showing a modification of the MoO₃/BHJ interface.

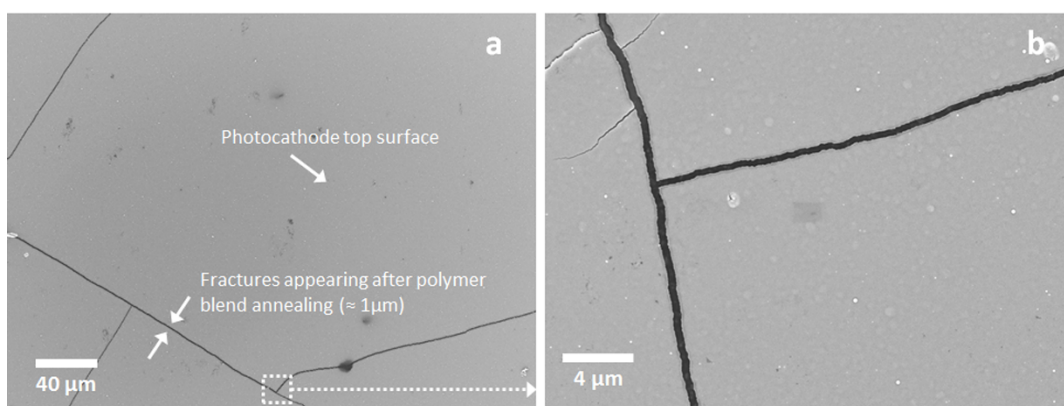


Figure S7. HR-SEM micrographs (top view) of the photocathode top surface showing the fracture lines appearing in the structure after polymers blend annealing procedure (10minutes at 130°C in N₂ atmosphere). Figure S3a and S3b show the surface at different magnifications.

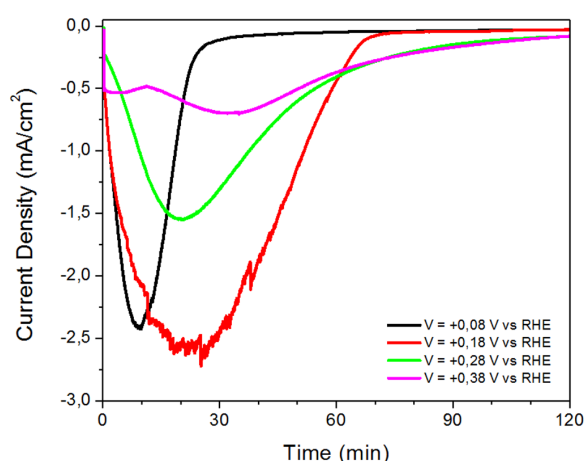


Figure S8. Evolution of the chronoamperogram with applied bias voltage under AM1.5 illumination for FTO/MoO₃/BHJ/TiO₂/Pt architecture. Note the evolution of the magnitude and the temporal position of the peak current density while the device is biased towards more negative voltages.

The evolution of the chronoamperometric signal showed in figure SI4 is characterized by an improvement and degradation phase as a function of the operation time. The initial raise in current density will be commented later in relation with J-V data. The existence of a current density maximum and the following decrease phase are related to the modifications arising in the H_yMoO_x layer upon H⁺ cations intercalation. The permeation of the electrolyte down to the lower layers of the porous photocathode causes a progressively increasing cation intercalation, and hence molybdenum oxide reduction, while the device is operated in chronoamperometric mode. The intercalation process became faster when the devices are biased towards more negative potentials. After a certain operation time at a fixed bias the MoO₃ layer is likely to become heavily reduced leading to the formation of both low work-function MoO_{3-x}OH_x compounds and of metallic Mo(4+) centers corresponding to water-soluble MoO₂ compounds. The CA current density decreases probably owing to the disruption of the favorable energetic alignment at the molybdenum oxide/P3HT blend interface, as a result of the significantly lower work function.

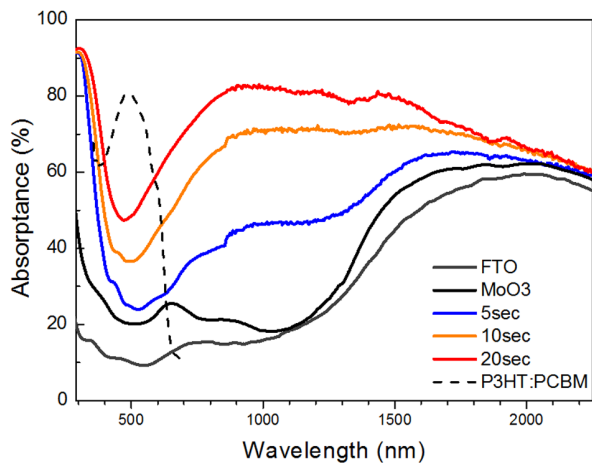


Figure S9. UV-Vis-nIR absorbance of FTO/ α -MoO₃ films intercalated in a pH 1.37 electrolyte buffer solution for different intercalation times at fixed bias potential of +0,18 V vs RHE. FTO substrate (grey solid line) and pristine FTO/ α -MoO₃ (black solid line) are plotted for reference. Black dashed line shows the absorption spectrum of FTO/BHJ sample.

The pristine FTO/ α -MoO₃ reference spectra shows two main features: the molybdenum oxide UV cut-off arising around 375 nm ($E_g = 3,3$ eV) and the IR plasmonic absorption of the FTO layer which is evident above 1250 nm. As deposited α -MoO₃ were 200 nm thick. Samples absorbance measured after electrochemical intercalation also exhibit a broad peak arising in the nIR-A region centered approximately around 1000 nm, which is interpreted as the plasmonic absorption of the MoO_{3-x}OH_x layer (black arrow). The central wavelength of the plasmonic peak, related via the plasma wavelength to the film free-carriers concentration, remains fixed around 1000 nm for different intercalation times while the magnitude of the absorbance increases. To explain this observations we note that while the H⁺ cations doping level, which mainly influences the film's n-type carrier concentration, is mainly controlled by the fixed bias intercalation voltage, the increasing absorbance as a function of immersion time is interpreted as a volume effect. For longer intercalation times increasingly deeper regions of the α -MoO₃ film can be reached by the electrolyte's cations and are progressively modified into MoO_{3-x}OH_x, giving raise to the characteristic blue coloration of molybdenum bronzes, this in turn enhances the intensity of the plasmonic absorbance peak. The formation of intercalated molybdenum oxide species deduced from absorbance spectra correlates well with the observed decrease in measured work functions on FTO/MoO₃ films electrochemically intercalated in similar experimental conditions shown in Figure 5c in the main text.

It is worth noting the close similarity between Figure SI5 absorptance spectrum of FTO/MoO₃ films which underwent electrochemical intercalation for 20 seconds and figure 5a (in the main text) absorptance spectrum of an FTO/ α -MoO₃/BHJ/TiO₂/Pt hydrogen evolution photocathode which underwent chronoamperometric measurements in the same buffer solution and with the same bias potential for 150 minutes. It is possible that the same mechanism of gradual intercalation happens during device's operation in CA mode with a much slower temporal dynamic, this delay can be explained taking into considerations the H⁺ cations diffusion and electrolyte infiltration barrier effect introduced by the BHJ/TiO₂/Pt overlayer in the full photocathode configuration.

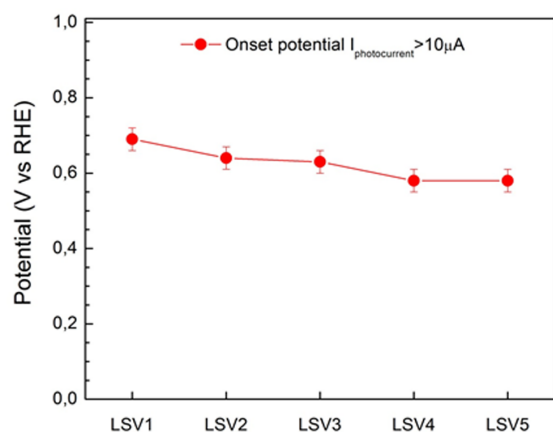


Figure S10. Variation of the onset potential (OP, potential at which the generated photocurrent exceed the 10 μ A threshold). Data are shown for five consecutive voltammetry scans. OCP's are defined as the voltage where the photocurrent density exceed 10 μ A/cm².

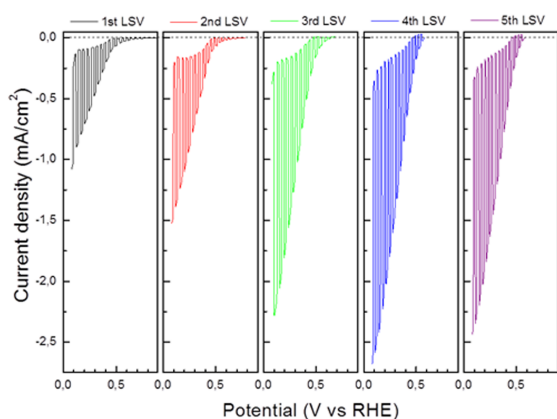


Figure S11. Evolution of the J–V characteristic in five consecutive voltammetric scans of FTO/MoO₃/BHJ/TiO₂/Pt photocathodes.

Figure S7 shows the evolution of J–V for consecutive voltammetry scans (scan rate 10 mV/sec from positive to negative voltages) under chopped AM1.5 illumination. Devices were biased at +0.18 V vs RHE and immersed in pH 1.37 electrolyte 1 M H₂SO₄-Na₂SO₄. Device architecture is FTO/MoO₃/BHJ/TiO₂/Pt.

The observed current density at positive bias and fill factor increase coupled with OCP decrease (Figure S6) over consecutive scans is qualitatively related to the evolution of the MoO₃ HSL layer work function. With reference to figure 1a and 5c in the main text the MoO₃/P3HT interface energy level alignment is progressively modified when the MoO₃ HSL layer incorporates H⁺ cations from the electrolyte over consecutive J-V. The formation of slightly sub-stoichiometric molybdenum oxide compounds (MoO_{3-x}OH_x) compounds, where a small fraction of the Mo atoms are reduced to Mo(5+) states, suggests a device operating with a reduced contact resistance and improved hole transport through shallow conduction band gap states. This phenomenon is likely reflected in the large enhancement of both the current density at positive bias and the FF. However, as the intercalation process proceeds during device operation, the progressive formation of higher amount of reduced Mo(5+) states also disrupts the initially favorable energy levels alignment at the MoO_{3-x}OH_x/P3HT interface. The decreased work function of the MoO_{3-x}OH_x which is pinned to the P3HT HOMO might explain the decrease of the overall current density OCP of the device over consecutive J-V scans as it is seen in Figure S6 and S7.

The trade-off in between the the two mechanisms described after Figure S4, S6 and S7 and the reduction kinetic of the MoO₃ reactions upon H⁺ intercalation determines the temporal position as well as the maximum magnitude of the photocathode's current density shown in Figure S4 and S7.